HHS Public Access

Author manuscript

Mol Cancer Res. Author manuscript; available in PMC 2024 July 02.

Published in final edited form as:

Mol Cancer Res. 2024 January 02; 22(1): 41–54. doi:10.1158/1541-7786.MCR-23-0512.

RNF185 control of COL3A1 expression limits prostate cancer migration and metastatic potential

Benjamin Van Espen[1], **Htoo Zarni Oo**[2], **Colin Collins**[2], **Ladan Fazli**[2], **Alfredo Molinolo**[3], **Kevin Yip**[1], **Rabi Murad**[1], **Martin Gleave**[2], **Ze'ev A. Ronai**[1]

[1]Cancer Center, Sanford Burnham Prebys Medical Discovery Institute, La Jolla, CA 92037, USA

[2]Vancouver Prostate Centre, Department of Urologic Sciences, University of British Columbia, Vancouver, BC V6H 3Z6, Canada

[3]Department of Pathology, The University of California San Diego, La Jolla CA, 92037.

Abstract

RNF185 is a RING finger domain-containing ubiquitin ligase implicated in ER-associated degradation. Prostate tumor patient data analysis revealed a negative correlation between RNF185 expression and prostate cancer progression and metastasis. Likewise, several prostate cancer cell lines exhibited greater migration and invasion capabilities in culture upon RNF185 depletion. Subcutaneous inoculation of mouse prostate cancer MPC3 cells stably expressing shRNA against RNF185 into mice resulted in larger tumors and more frequent lung metastases. RNA-sequencing and Ingenuity Pathway Analysis identified wound healing and cellular movement among the most significant pathways upregulated in RNF185-depleted, compared to control prostate cancer cells. Gene Set Enrichment Analyses performed in samples from patients harboring low RNF185 expression and in RNF185-depleted lines confirmed the deregulation of genes implicated in EMT. Among those, COL3A1 was identified as the primary mediator of RNF185's ability to impact migration phenotypes. Correspondingly, enhanced migration and metastasis of RNF185 KD prostate cancer cells were attenuated upon co-inhibition of COL3A1. Our results identify RNF185 as a gatekeeper of prostate cancer metastasis, partly *via* its control of COL3A1 availability.

Keywords

ubiquitin ligase; RNF185; prostate adenocarcinoma; metastasis; epithelial-mesenchymal transition (EMT); collagen

Correspondence: Ze'ev A Ronai, Cancer Center, SBP Discovery, 10901 N. Torrey Pines Road, La Jolla, CA, 92037. zeev@ronailab.net.

Author Contributions

BVE and ZAR designed the study. BVE performed the experiments. AM performed pathological assessments. LF, HZO and RM performed bioinformatic analyses. MG provided clinical samples. BVE and ZAR wrote the manuscript.

Authors Disclosure: Ze'ev A Ronai is a co-founder and scientific advisor of Pangea Biomed. All other authors have nothing to declare.

Introduction

Prostate cancer (PCa) is among the most common solid malignancies in developed regions and the second most common in men worldwide (1). While most PCa are not life-threatening, a sizeable fraction of primary PCa progresses to advanced disease; as a result, PCa is the second leading cause of cancer death in American men (2). Advanced PCa often harbors amplification and/or mutation of the androgen receptor (AR), making Androgen Deprivation Therapy (ADT) the primary treatment regime. However, most patients eventually develop resistance to ADT and progress to metastatic disease, known as metastatic Castration-Resistant Prostate Cancer (mCRPC). Once tumors become castration-resistant, the prognosis is bleak, as this form of PCa is considered incurable (3). Whereas disease trajectory can be somewhat predicted based on histopathological and molecular profiling, reliable markers of prostate cancer progression and therapeutic targets for mCRPC remains a major unmet clinical need (4).

Ubiquitination is a post-translational modification in which a ubiquitin moiety is added to lysine residues of target proteins, enabling the formation of ubiquitin chains of different topologies (5). Those modifications can alter protein localization and complex formation or result in proteasome-mediated degradation of the target protein. While dysregulation of the ubiquitin system is often implicated in birth defects, neurodegenerative disease, and tumorigenesis (6, 7), the impact of E3 ligase dysregulation is context-dependent. For example, increased expression of the ubiquitin ligase RNF5 is seen in several human cancers but has different outcomes for breast cancer, melanoma, or acute myeloid leukemia (8–10).

Growing evidence points to a role for the RNF5-closely related ubiquitin ligase RNF185 in endoplasmic reticulum-associated degradation (ERAD), a process essential for cellular protein homeostasis. Notably, RNF185 is implicated in cellular functions linked to RNF5 (11–17). The two proteins share >70% sequence identity, and, as seen for RNF5, RNF185 dysregulation reportedly impacts diverse cancer types (18, 19).

Proteins of the collagen family reportedly play critical roles in diverse cellular processes, including cell adhesion, migration, differentiation, and proliferation (20). Correspondingly, collagen dysregulation is implicated in several pathologies, including cancer (21–23). COL3A1 (collagen type III alpha 1) is one of the main collagen types expressed in stromal cells and is mainly produced by fibroblasts, as such, it contributes to regulating the tumor microenvironment (TME) (24, 25). COL3A1 mRNA expression is upregulated in various cancer subtypes, including breast, lung, head and neck, pancreatic, ovarian, gastric, esophageal cancers, and glioma (26–31). Moreover, high COL3A1 expression is often associated with increased tumor growth, invasion, metastasis, and sometimes therapy resistance (32–35).

Here we identify an important function for RNF185 in PCa migration and metastatic behavior and report that COL3A1 mediates these effects. Overall, our findings establish RNF185 as functioning in the regulation of COL3A1 levels, an activity that impacts the progression and metastasis of prostate cancer.

Material & Methods

Animal studies

All mouse studies were approved by Sanford Burnham Prebys (SBP) IACUC protocol # 20–064. The xenograft model was established using MPC3 cells expressing either control shRNA or shRNA targeting RNF185, COL3A1 or both using the PLKO-1 vector. NOD/SCID/Gamma (NSG) mice were obtained from the SBP Animal Facility. Eight-week-old male mice were injected subcutaneously in the flank with 5×10^5 cells. Mice were housed four per cage and maintained under controlled temperature (22.5°C) and illumination (12 h dark/light cycles) conditions. Mice were sacrificed upon signs of morbidity resulting from tumor growth or if maximal tumor size/burden (2 cm^3) was reached. Tumor volume was measured with linear calipers and calculated using the formula: (length in mm × width in mm) × 1/2. After mice were sacrificed, tumors and lungs were snap-frozen and later utilized for histopathological analysis. Fixed and embedded lung tissues were sliced into 5 μm sections to obtain nine serial sections per lung. Metastases in the lungs were evaluated by hematoxylin and eosin staining and quantified in a total of 9 serial sections for each mouse, using ImageScope v12.3.3 (APERIO, RRID: SCR_014311). The average metastatic area (mm^3) per section was reported for each group.

Cell lines and cell culture

Hek293T human kidney epithelial cells (ATCC Cat# CRL-3216, RRID: CVCL_0063) and PCa lines PC3 (ATCC Cat# CRL-1435, RRID: CVCL_0035), C4–2B (ATCC Cat# CRL-3315, RRID:CVCL_4784), TRAMP-C2 (ATCC Cat# CRL-2731, RRID:CVCL_3615) and MyC-CaP (ATCC Cat# CRL-3255, RRID: CVCL_J703)) were obtained from the American Type Culture Collection (ATCC). MPC3 cells were kindly provided by Prof. Zhenbang Chen. PC3 and C4–2B cells were cultured in RPMI growth medium [RPMI supplemented with 10% fetal bovine serum (FBS; Omega Scientific) and 100 units penicillin/mL and 100 units streptomycin/mL]. Hek293T and the mouse PCa line MPC3, TRAMP-C2 and MyC-CaP were cultured in DMEM growth medium (DMEM supplemented with 10% FBS and 100 units penicillin/mL and 100 units streptomycin/mL). Cells were maintained at all times in growth phase. All cell lines tested negative for mycoplasma contamination with MycoAlert® Mycoplasma Detection Kit (Lonza, LT07–118).

RNA isolation and quantitative reverse transcription PCR (RT-qPCR)

Total RNA was extracted from cells using a GenElute RNA purification kit (Sigma-Aldrich, RTN70). RNA purity and concentration were assessed using a NanoDrop spectrophotometer (Thermo Fisher). Aliquots of 1 ug of total RNA were reverse transcribed using qScript cDNA synthesis kit (Quantabio, 95047–500) according to the manufacturer's protocol. qRT-PCR analyses were performed using LightCycler® 480 SYBR Green I Master RT-PCR kits (ROCHE) on a Bio-Rad CFX Connect Real-Time system (Bio-Rad, CFX Connect Real-Time System). Expression levels were normalized to GAPDH. Sequences of oligonucleotide primers were as follows; mouse Rnf185 forward (5′- GCAGACCTATCAATCAACGCC-3') and reverse (5′-CGAAGGCCCTTTACTTGCCAT-3′); mouse Gapdh forward (5′-AGGTCGGTGTGAACGGATTTG-3') and reverse (5′- TGTAGACCATGTAGTTGAGGTCA-3′); mouse

Col3a1 forward (5′-CTGTAACATGGAAACTGGGGAAA-3’) and reverse (5′-CCATAGCTGAACTGAAAACCACC-3′); mouse Col5a2 forward (5′-TTGGAAACCTTCTCCATGTCAGA-3’) and reverse (5′-TCCCCAGTGGGTGTTATAGGA-3′); human RNF185 forward (5′-GGAGAATAGAGGGGGATTTC-3’) and reverse (5′-AAATGCTGTGGCAAATAT-3′); human GAPDH Forward (5′-GGAGGGAGATCCCTCCAAAAT-3’) and reverse (5′-GGCTGTTGTCATACTTCTCATGG-3′); human COL3A1 forward (5′-GGAGCTGGCTACTTCTCGC-3’) and reverse (5′-GGGAACATCCTCCTTCAACAG-3′); human COL5A2 forward (5′-GACTGTGCCGACCCTGTAAC-3’) and reverse (5′-CCTGGACGACCACGTATGC-3′).

Western blot analysis

Cells were washed twice with PBS at room temperature and resuspended in lysis buffer [100 mM Tris-HCl pH 7.5, 5% sodium dodecyl sulfate (SDS)]. Lysates were boiled 10 minutes and then sonicated with a Microtip sonicator and separated by SDS-PAGE. Proteins were transferred to nitrocellulose membranes (Bio-Rad, 1704159). Membranes were blocked in 5% skim milk and incubated with respective primary antibodies followed by HRP-conjugated secondary antibodies (Jackson ImmunoResearch Labs Cat# 111-035-045, RRID: AB_2337938 and Cat# 115-035-062, RRID: AB_2338504). Blots were imaged with a ChemiDoc imaging system (Bio-Rad, ChemiDoc MP imaging system) using ECL Western blotting HRP substrate (Millipore, WBLUR0500).

Antibodies and chemicals

Antibodies were obtained from the following sources: RNF185 (181999, Abcam, RRID: AB_2922962); β-Tubulin (2128, Cell Signaling Technology, RRID: AB_823664); SMAD2 (5339, Cell Signaling Technology, RRID:AB_10626777); phospho-SMAD2 (3108, Cell Signaling Technology, RRID:AB_490941); SMAD3 (9523, Cell Signaling Technology, RRID:AB_2193182); phosphor-SMAD3 (9520, Cell Signaling Technology, RRID:AB_2193207); SMAD4 (38454, Cell Signaling Technology, RRID:AB_2728776); HRP-conjugated secondary antibodies: goat-anti-mouse-HRP (Jackson ImmunoResearch, Cat# 115-035-062, RRID: AB_2338504) and goat-anti-rabbit-HRP (Jackson ImmunoResearch, Cat# 111-035-045, RRID: AB_2337938). Antibodies were used at a dilution of 1:1000, and blots were washed 3 times with TBST before being incubated with secondary antibodies at a dilution of 1:10000.

Plasmids, short interfering RNA (siRNA), short hairpin RNA (shRNA) and lentiviral infection

For transient gene depletion, oligonucleotide siRNAs targeting RNF185, COL3A1 and COL5A2, and siRNA Universal Negative Control were purchased from MISSION® Predesigned siRNA libraries (Sigma-Aldrich). Cells were transfected using JetPRIME transfection reagents (PolyPlus, 101000015). Experiments were performed at 24h or 48h post-transfection. For stable RNF185 overexpression, RNF185 WT sequence was cloned into pLX304 vector containing C-terminal v5-tag, using the pENTR™/D-TOPO™ Cloning Kit (Invitrogen). pLX304 empty vector was used as negative control. The lentiviral pLKO.1 vector was used to introduce short hairpin RNA (shRNA) targeting RNF185, COL3A1 or

the scramble control into MPC3 cells. Sequences for shRNAs were identified through the MISSION® Predesigned shRNA libraries (Sigma-Aldrich) and shRNAs were obtained from the La Jolla Institute for Immunology RNAi Center (La Jolla, CA, USA). pLX304 empty vector, pLX304.RNF185-v5, pLKO.shRNF185, pLKO.shCOL3A1 and pLKO.scramble infectious lentiviral stocks were generated in Hek293T cells. MPC3 cells were infected 8 h with lentivirus in the presence of 8 μg/mL polybrene (Millipore). After 48 h, cells stably expressing scramble, targeted shRNA(s) or RNF185-v5 were selected in 2 μg/mL puromycin or 5 μg/mL blasticidin for the latter. Five days later, antibiotic concentration was halved. Antibiotic treatment was stopped 48 h before beginning experimental procedures.

LC-MS/MS

For full proteome analysis of RNF185 KD cells, MPC3 cells stably expressing pLKO empty vector (control) or shRNA against RNF185 were lysed in 100 uL TNE lysis buffer (150 mM Tris-HCl pH 7.5, 150 Mm NaCl, 0.5 mM EDTA, protease and phosphatase inhibitor cocktail). Samples were processed for LC-MS/MS analysis as described below.

S-Trap mini columns (Protifi, K02-mini) were used for protein digestion. Samples were analyzed by LC-MS/MS using a Proxeon EASY-nanoLC system (ThermoFisher) coupled to an Orbitrap Fusion Lumos Tribid mass spectrometer (Thermo Fisher Scientific). All mass spectra were analyzed with MaxQuant software version 1.6.11.0. MS/MS spectra were searched against the Mus musculus Uniprot protein sequence database, and GPM cRAP sequences.

Total proteomics analysis was performed in R version 4.2.1 and MSstats version 4.4.1 (36). MaxQuant processed files were converted to MSstats format using MaxQtoMSstatsFormat. Data was normalized using dataProcess with default parameters. shRnf185 versus Plko differential expression comparison was performed using limma package's lmfit and eBayes functions (37).

Cell proliferation assay

Cells were plated in 96-well clear-bottomed plates (Corning, 3610) at a density of 2,000 cells/100 μL of medium per well. Proliferation was measured every 24h by treating cells with 30 μL of the CellTiter Glo kit reagent (Promega) and measuring luminescence with a CLARIOstar Plus microplate reader (BMG Labtech).

Cell migration and invasion assay (Boyden chamber)

Transwell plates were obtained from Corning (#3342). For migration assays, 2×10^4 cells of the MPC3, MyC-CaP and TRAMP-C2 lines and 6×10^4 cells of PC3 and C4–2B lines were seeded into the upper chamber in 100 μL serum-free medium. The lower chamber was filled with 600 μL of medium supplemented with 10% FBS as a chemo-attractant. After incubations of 24h or 48h (C4–2B), cells were fixed in 4% PFA and stained with 0.5% crystal violet. Cells on the upper surface of the filter were removed with a cotton swab. For quantification, crystal violet stain was eluted by incubating inserts in 30% acetic acid, and absorbance was measured at 492 nm using a CLARIOstar Plus microplate reader (BMG

Labtech). For invasion assays, Transwells were first coated with Matrigel overnight, and then procedures described for the migration assay were followed.

Spheroid formation assay

Cells were plated in Nunc™ MicroWell™ MiniTrays (ThermoFisher # 438733) at a density of 200 cells/20 μL of medium per well. The tray was then flipped upside-down to allow cells to grow in hanging droplets and form 3D spheroids in which cells are in direct contact with each other and with extracellular matrix components. The trays were placed in 150 mm tissue culture dish with 5 mL of PBS and a piece of Whatman filter paper to act as hydration chamber. Spheroids size was measured after 3, 5 and 9 days of incubation. For quantification, either pictures of each spheroid were processed with ImageJ (RRID:SCR_003070), where surface areas occupied by spheroids were measured, or proliferation was evaluated using CellTiter Glo 3D kit reagent (Promega) and luminescence measurement with a CLARIOstar Plus microplate reader (BMG Labtech).

RNA-seq library construction

PolyA RNA was isolated using NEBNext® Poly(A) mRNA Magnetic Isolation Module, and bar-coded libraries were constructed using the NEBNext® Ultra™ Directional RNA Library Prep Kit for Illumina® (NEB, Ipswich MA). Libraries were pooled and sequenced single-end (1X75) on an Illumina NextSeq 500 using the High output V2 kit (Illumina Inc., San Diego CA).

RNA-seq processing and analysis

Raw sequencing reads were pre-processed to remove llumina Truseq adapters and polyA/polyT sequences using Cutadapt version 2.3 (38). Trimmed reads were aligned against mouse genome version mm10 and Ensembl gene annotations version 84 using STAR version 2.7.0d_0221 (RRID:SCR_004463) (39), and alignment parameters from ENCODE long RNA-seq pipeline (https://github.com/ENCODE-DCC/long-rna-seq-pipeline). Gene level estimated counts and transcripts per million (TPM) were obtained using RSEM version 1.3.1 (40). FastQC version 0.11.5 (https://www.bioinformatics.babraham.ac.uk/projects/fastqc/; RRID: SCR_014583) and MultiQC version 1.8 were used to assess the quality of trimmed reads and alignment to genome/transcriptome (41). Batch effect correction was performed using *Combat_seq* function in sva version 3.44.0. The sequencing libraries were built in three batches: batch1 contained replicates 1 and 2 of each condition, batch 2 contained replicates 3 and 4, and batch 3 contained replicates 5 and 6. Differential expression comparisons were performed using batch-corrected counts and Wald test implemented in DESeq2 version 1.22.2 (RRID: SCR_000154) (42). Genes with Benjamini-Hochberg corrected p-value < 0.05 and log2 fold change ≥ 1.5, or ≤ -1.5 were identified as differentially expressed. Counts per million (CPM) and reads per kilobase per million (RPKM) values were computed from batch-corrected counts using edgeR version 3.38.4 (RRID: SCR_012802) (43). Gene lengths (sum of exon lengths) for RPKM calculation were computed from Ensembl gene annotations version 84 GTF file using GenomicsFeatures Bioconductor package version 1.48.4 (RRID: SCR_006442) (44). Gene set enrichment analysis (GSEA) for TCGA-PRAD comparison of RNF185 low versus high expressors was performed using preranked option in GSEA version 4.2.3 (RRID: SCR_003199) (45).

GSEA for RNA-seq comparisons were performed using GSEA version 4.3.2 and RPKM values with parameter “Permutation type = gene_set”. Pathway analysis was performed using Ingenuity Pathway Analysis (Qiagen, Redwood City, USA; RRID: SCR_008653).

Analysis of clinical databases

Clinical samples from the Taylor et al. prostate adenocarcinoma cohort (46) and The Cancer Genome Atlas (TCGA) Pan-Cancer prostate adenocarcinoma (PRAD) dataset (47) were used. Gene expression and clinical annotation were downloaded from cBioPortal Cancer Genomic Portal (http://cbioportal.org) (48). The bottom and top quartiles were used to identify mRNA expression higher or lower than normal prostate samples. The Kaplan–Meier method was used for disease-free survival analysis. For comparison of RNF185 and COL3A1 mRNA expression in samples stratified by Gleason score and by sample type (primary vs. metastasis), the log2 (fold-change) value was used.

Statistical analysis

At least 3 samples were used in each experimental group. All experiments were performed at least three times to establish statistical power and reproducibility. Differences between two groups were assessed using two-tailed unpaired t-tests or Mann-Whitney u test. One-way ANOVA with Tukey’s multiple comparison test was used to evaluate experiments involving one factor but multiple groups. Two-way ANOVA with Tukey’s multiple comparison test was used to evaluate experiments involving two factors and multiple groups. Fisher’s exact test was used to analyze 2×2 contingency table of small sample size. Disease-free survival was analyzed by the Kaplan–Meier method and evaluated with a log-rank (Mantel-Cox) test. All analyses were performed using GraphPad Prism software (RRID: SCR_002798). $P < 0.05$ was considered significant. We have used the hypergeometric test for Venn diagrams comparing the overlapping differentially expressed genes in MPC3.shRNF185#1 and MPC3.shRNF185#3. The total number of expressed genes in MPC3.shRNF185#1 vs. MPC3.plko and MPC3.shRNF185#3 vs. MPC3.plko were 15,404 and 15,480 respectively. For the hypergeometric test of overlap significance, we used the total number of common genes (n=15279) in both comparisons as the total number of genes. We used R version 4.2.1 hypergeometric test function phyper(q, m, n, k, lower.tail = FALSE, log.p = FALSE) to compute p-value of overlap, where q = (size of overlap – 1), m = number of DE genes in comparison 1, n = total number of genes, and k = number of DE genes in comparison 2.

Data Availability

Data analyzed in this study were obtained from cBioPortal Cancer Genomic Portal (http://cbioportal.org) (48). Raw and processed RNAseq data have been deposited at Gene Expression Ominibus GEO under accession GSE228999. Raw data generated in this study were generated using immunohistochemistry, Western blots and qPCR analyses, and all are available upon request from the corresponding author. The mass spectrometry proteomics data have been deposited to the ProteomeXchange Consortium via the PRIDE (49) partner repository with the dataset identifier PXD045473.

Results

Low RNF185 expression correlates with metastatic load and unfavorable PCa patient outcomes.

Analysis of RNF185 mRNA levels in independent cohorts of PCa patients revealed that low RNF185 mRNA expression was associated with poorer disease-free survival in the prostate adenocarcinoma (PRAD) dataset from The Cancer Genome Atlas (TCGA) (47). Consistently, analysis of an independent patient cohort consisting of ~218 human prostate tumors (181 primary tumors and 37 metastases) revealed that low RNF185 expression coincided with poorer prognosis (46). Median disease-free survival was 53.82 months in RNF185-low samples and undefined (survival >50% at the longest time-point) in all others. In the RNF185-low expressing group, 13 of 24 (54.2%) progressed, whereas 19 of 88 (21.6%) progressed in the RNF185-high expressing group (Fig. 1A). Notably, 52.94% of RNF185-low expressing samples were metastatic compared with 5.2% in the RNF185-high expressing group (Fig. 1B). Likewise, metastatic samples showed significantly lower RNF185 mRNA expression than non-metastatic samples (Fig. 1C). To confirm that lower RNF185 mRNA levels are associated with poorer prognosis, we examined RNF185 expression in samples stratified based on Gleason grade, a histopathological measure of prostate tumor stage and aggressiveness. RNF185 expression in high Gleason grade tumors was significantly lower relative to intermediate and low Gleason grade tumors. (Fig. 1D). In TCGA's PRAD dataset, samples with low RNF185 mRNA levels also correlated with poor disease-free survival, with a median of 45.24 disease-free months compared to a >50% disease-free survival rate associated with higher RNF185 expression. In the RNF185-low expressing group, 12 of 32 (37.5%) progressed compared with 17 of 299 (5.7%) in the RNF185-high expressing group (Fig. 1E). Lower RNF185 mRNA levels were also associated with higher Gleason grade, shorter progression-free survival, increased new neoplastic events post initial therapy, greater lymph node involvement and higher tumor stage in that dataset (Fig. 1F, Supp. Fig. 1A–D).

Further assessment carried out using an independent patient cohort (VPC) revealed a negative correlation between RNF185 expression and overall survival (Fig. 1G). Lower RNF185 expression was confirmed in patients with higher Gleason grades (Fig. 1H), with metastases (Fig. 1I), and with more advanced pathological stages (Fig. 1J). Overall, patients considered at high risk exhibited lower RNF185 mRNA expression (Supp. Fig. 1E).

Given that RNF185 is a ubiquitin ligase, its abundance, subcellular localization, and/or activity could be altered by self-degradation and post-translational modification. Therefore, RNF185 transcript levels may not reflect its activity. Evaluation of RNF185 protein levels by immunohistochemistry (IHC) staining of a tissue microarray (TMA) derived from PCa patients revealed a significant decrease of RNF185 staining intensity in samples assigned with the highest Gleason groups: the RNF185 IHC score was significantly lower in samples from Gleason group 5 (high risk) relative to samples from Gleason groups 3 and 4 (intermediate risk) (Fig.1K). Weaker RNF185 staining intensity also correlated with higher percentage of recurrence (Supp. Fig. 1F). These observations, using 3 independent patient cohorts, establish that RNF185 expression (at both transcript and protein levels)

inversely correlates with advanced PCa stage (Gleason grade), propensity to metastasize and decreased overall survival.

RNF185 KD enhances PCa cell migration, tumor development and metastatic load.

The relationship between RNF185 mRNA levels and unfavorable patient outcomes prompted us to test the effect of altering RNF185 expression in PCa-derived cell lines, both *in vitro* and *in vivo*. To this end, we infected the mouse PCa line MPC3 (*Pten*$^{-/-}$*::p53*$^{-/-}$) (50, 51) with lentivirus expressing control shRNA or shRNF185. MPC3 cells stably expressing shRNF185, confirmed to express low levels of RNF185 (RNF185 KD), were selected (Fig. 2A), and monitored for potential changes in migration and invasion. RNF185 KD MPC3 cells exhibited significantly greater migration and invasion capacity compared with control shRNA cells (Fig. 2B–C). RNF185 depletion also increased anchorage-independent growth measured by spheroid formation assay (Sup. Fig, 2A). In contrast, RNF185 KD did not alter proliferation of cells, grown under two-dimensional conditions (Fig. 2D). Interestingly, the effect of RNF185 KD on migration seen in MPC3 cells was not observed in mouse prostate cancer cell lines TRAMP-C2 and MyC-CaP, which harbor different mutations (52, 53) (Supp. Fig. 2B–G), implying that select genetic drivers of PCa could impact the ability of RNF185 to alter PCa phenotypes. One common alteration in these responsive lines was PTEN deletion, which is known to be associated with advanced stages of prostate cancer (3, 54, 55). Analysis of clinical attributes, based on PTEN CNAs and RNF185 expression, revealed that a higher proportion of metastatic samples in patients with low RNF185 and PTEN deletion compared to those with low RNF185 and intact PTEN copies or high RNF185 expression with PTEN deletion (Sup. Fig. 2I). Furthermore, patients with both PTEN deletion and low RNF185 expression had worse prognoses than those with either low RNF185 expression or PTEN deletion alone (Sup. Fig. 2H). Notably, very few patients presented high RNF185 expression while harboring PTEN deletion, suggesting a link between the two events.

To monitor possible changes in MPC3 cell metastatic propensity *in vivo*, we inoculated NSG mice subcutaneously with RNF185 KD or control cells. Larger tumors were observed in mice inoculated with RNF185 KD as compared to WT MPC3 cells (Fig. 2E, Supp. Fig.2J–K). Notably, 7 of 20 mice inoculated with RNF185 KD cells developed lung metastases (a total of 13 micro-metastases were detected) compared with 1 of 20 in the control MPC3 tumor cohort (only 1 micro-metastasis detected). These observations are consistent with enhanced migration phenotypes seen in cultured MPC3 cells (Fig. 2F). Enhanced migratory capability upon RNF185 knock-down was validated in cultures of human prostate cancer lines PC3 and C4–2B (Fig. 2G–H). Both lines also formed larger spheroids upon RNF185 inhibition (Supp. Fig. 2L–M). As an additional validation of RNF185's role in PCa cells motility, we performed a migration assay in MPC3 cells overexpressing RNF185. As expected, RNF185 overexpression reduced migration in MPC3 cells (Sup. Fig. 2N). Furthermore, we interrogated RNF185 basal protein expression in the cell lines we used for migration assay and found that RNF185 basal protein level correlates with how fast cells migrated in our assays (Sup. Fig. 2O). The cell line with greater baseline migratory capabilities (TRAMP-C2 and Myc-CaP) had lower RNF185 protein abundance compared to the slowest line (C4–2B). These analyses demonstrate that RNF185 plays a role in PCa

motility and that manipulation of RNF185 expression can influence the metastatic potential of select prostate cancer cells.

Transcriptional analysis suggests activation of the Epithelial-to-Mesenchymal Transition and collagen upregulation in RNF185 KD cells.

To identify possible mechanisms underlying RNF185's effect on cell migration, we performed RNA-seq analysis of RNF185 KD and control MPC3 lines. Gene expression analysis was performed using six replicate samples of MPC3 cells expressing one of two different shRNAs (shRNF185 #1 and #3) compared with control shRNA-infected cells. Analysis of differentially-expressed genes (DEGs) revealed clustering that distinguished the control from the two RNF185 KD lines (Fig. 3A). Even though shRNF185#1 and shRNF185#3 clustered separately in the Principal Component Analysis, Ingenuity Pathway Analysis (IPA) yielded similar results in both groups when compared to controls. In both cases IPA identified gene clusters representing cellular movement/migration as upregulated, coinciding with phenotypic changes seen in RNF185 KD MPC3 cells (Fig. 3B). Furthermore, there was a significant overlap in up- or down-regulated genes between RNF185 KD lines #1 and #3 relative to controls (Supp. Fig. 3A). To identify potential drivers of migration phenotypes, we compared MPC3 cell RNA-seq data with clinically available transcriptomics data. Gene set enrichment analysis (GSEA) was first performed using differentially expressed gene lists from TCGA's PRAD dataset in which patients were clustered based on RNF185 mRNA expression (bottom 25% vs. top 25%). Next, we carried out GSEA analysis based on RNA-seq of RNF185-depleted MPC3 cells. Analysis of the Molecular Signatures Database (MSigDB) identified a hallmark gene set enriched for factors associated with the Epithelial-to-Mesenchymal Transition (EMT) (Fig. 3C, Supp. Table 1–3) (56). Based on the GSEA results, a list of select genes driving the enrichment score and common to all datasets was generated and used for independent validation (Fig. 3D–E, Supp. Fig. 3B). This list included a number of shared genes encoding fibrillar collagens that were identified as potential drivers. Among these, upregulation of COL3A1 and COL5A2, upon RNF185 KD, was validated in both mouse and human lines (Fig. 3E).

Prior studies have established that RNF185 functions as an ER-associated E3 ligase implicated in ER stress response and protein quality control (57). RNF185 contributes to ER quality control by orchestrating the ubiquitin-proteasome-mediated degradation of misfolded proteins, including the cystic fibrosis transmembrane conductance regulator (CFTR) and CFTRΔF508 mutant (15). It was also shown to form a complex with TMUB1/2, TMEM259/Membralin (MBRL), and UBE3C, involved in recognizing, ubiquitinating, and degrading specific ER membrane substrates (58). This complex cooperates with UBE3C and the p97 ATPase to extract ubiquitinated substrates from the ER membrane for proteasomal degradation. The interaction between RNF185 and the ERAD factor p97 underscores its role in coordinating cellular proteostasis. Therefore, we have interrogated changes in protein expression following inhibition of RNF185 expression in the MPC3 line. Proteomics analysis of MPC3 lysate from RNF185 KD cells using LC-MS/MS identified upregulation of proteins implicated in EMT, cell migration, including COL3A1, COL1A1, MMP14, SERPINH1, FN1, LAMA5 (Sup. Fig. 3E), corroborating our RNA-seq analysis. Interestingly, the changes observed at the protein level in MPC3-KD cells resembled gene

expression signatures associated with invasive squamous cell carcinoma and progression to metastatic disease in pancreatic cancer (59, 60). Interestingly, SERPINH1, which was previously established as a prognostic biomarker in 14 different cancer types, correlating with anti-tumor immunity and regulation of the TME, including collagen synthesis (61), was also upregulated upon RNF185 KD. SERPINH1 has been implicated as a key modulator of EMT, via the Wnt/β-catenin pathway, in gastric cancer (62), and was shown to regulate collagen triple-helical structure stability and promote changes in the TME associated with reduced immune infiltration and increased metastases in lung adenocarcinoma (63). Overall, the changes observed at the protein level in RNF185 depleted cells correlated with the Hallmark of EMT signature from MSigDB (Sup. Fig.3F). Taken together, our transcriptomics and proteomics analysis of RNF185-KD cells point to the activation of EMT and changes in fibrillar collagens, with COL3A1 and COL5A2 being the most consistently upregulated (Fig. 3E). Accordingly, we have selected COL3A1 and COL5A2 for further evaluation.

COL3A1 drives enhanced migration in vitro and in vivo and correlates with unfavorable patient prognosis.

To directly assess whether changes seen upon RNF185 KD are mediated by upregulation of COL3A1 or COL5A2, we performed rescue experiments in PC3 cells. Each of these genes was inhibited, using the corresponding siRNA, individually or together with RNF185, followed by monitoring possible changes in cell migration. Inhibition of COL3A1 had no effect on migration, while inhibition of COL5A2 increased migration. Notably, however, inhibition of COL3A1 in RNF185 KD cells was sufficient to attenuate the increased migration seen upon RNF185 KD. Conversely, inhibition of COL5A2 did not affect the migration phenotypes seen following RNF185 KD (Fig. 4A–B). As expected, inhibition of both COL3A1 and COL5A2 in RNF185 KD cells also rescued migration phenotypes, which was seen by KD of COL3A1 alone (Fig. 4A–B). Interestingly, COL5A2 depletion induced COL3A1 upregulation and vice versa (Supp. Fig. 4A–C), suggesting a possible cross talk that links their expression. Consistent with these observations, analysis of patient samples from the Taylor et al. dataset (46) revealed that high COL3A1 expression coincided with poorer prognosis. In the COL3A1-high group, 17 of 33 (51.5%) progressed, whereas only 3 of 36 (8.3%) progressed in the COL3A1-low group (Fig. 4C). COL3A1 expression in high Gleason grade tumors was significantly greater than in intermediate and lower Gleason grade tumors (Supp. Fig. 4D). Along these lines, mRNA expression of RNF185 and COL3A1 were found to be negatively correlated in the TCGA PRAD dataset (Fig. 4D). Analyses of independent PCa datasets (from VPC) revealed that COL3A1 expression was primarily seen in patients with higher Gleason grades (Fig. 4E), with a more advanced pathological stages (Fig. 4F), and with more metastases (Fig. 4G). Overall, patients considered at high risk exhibited higher COL3A1 mRNA expression (Fig. 4H). A positive correlation between COL3A1 expression and PSA recurrence was also observed in this patient cohort (Fig. 4I).

To validate these findings *in vivo*, we established stable MPC3 cells expressing shRNA against RNF185, COL3A1, and a combination of both (Supp. Fig. 5A–B). The increased migration and invasion phenotypes previously seen upon RFN185 KD, as well as the rescue

of this phenotype in the RNF185/COL3A1 double KD, were confirmed in the Boyden chamber assay (Fig. 5A, Supp. Fig. 5C). Following this validation, RNF185 KD, COL3A1 KD, RNF185/COL3A1 double KD, and control MPC3 cells were inoculated subcutaneously in NSG mice. Analysis of tumor growth revealed significantly larger tumors in the RNF185 KD inoculated mice compared to the control group, as shown in earlier experiments (Fig. 2E, Supp. Fig.2H). Notably, COL3A1 KD in combination with RNF185 KD effectively attenuated the effect of RNF185 KD alone, as mice inoculated with RNF185/COL3A1 double KD cells grew tumors of comparable size as the control group or mice inoculated with the COL3A1 KD cells (Fig. 5B–F). Quantification of lung metastasis identified that a wider area of the lungs inoculated with RNF185 KD cells contained metastases, when compared to the mice inoculated with the control cells, consistent with our earlier findings (Fig. 2F). Notably, COL3A1 depletion was sufficient to reduce the metastatic load seen upon inoculation with RNF185 KD cells; mice inoculated with tumors that were inhibited for both RNF185 and COL3A1 exhibited a metastatic load which was comparable with that seen in control mice. Interestingly, COL3A1 depletion on its own did not affect the number of lung metastases (Fig. 5G). These data suggest that COL3A1 upregulation underlies increased migration phenotype observed in RNF185-depleted cells, *in vitro* and *in vivo*, as depletion of COL3A1 is sufficient to attenuate the enhanced invasiveness of RNF185 KD prostate cancer cells.

Discussion

AR-dependent signaling is commonly dysregulated in prostate cancer, leading to transcriptional changes that promote cellular growth and functional outcomes associated with neoplasia. These activities provide a rationale for targeting androgen signaling, a goal accomplished in part through ADT therapy. Unfortunately, ADT frequently rewires AR signaling pathways in a way that promotes therapy resistance. Prostate cancer that develops ADT resistance usually progresses to mCRPC, for which the effective treatment remains limited (64). Here, we identify a role for the ubiquitin ligase RNF185 in prostate cancer progression and propensity to metastasize. Analyses of 3 independent prostate cancer patient datasets revealed that low RNF185 mRNA and protein expression was associated with poorer survival and higher Gleason grade and metastatic load. Notably, inhibition of RNF185 expression in mouse and human PCa lines increased invasive phenotypes in culture and resulted in larger tumors and increased lung metastases *in vivo*. Correspondingly, gene expression analyses identified enrichment of genes associated with cell migration and EMT, and pointed to the role of specific collagens in phenotypes seen in RNF185 KD PCa cells. Notably, the changes elicited upon RNF185 KD were seen in some but not all PCa cell lines tested, suggesting that certain genetic alterations are prerequisites to confer phenotypic changes when combined with the loss of RNF185. Our earlier observations on PTEN CNAs and RNF185 expression in patients suggest a potential synergistic effect of PTEN deletion and RNF185 downregulation on PCa progression, providing valuable insights into the complex interplay of genetic alterations in advanced stages of the disease. These observations may explain why cell lines with intact PTEN copies did not present any phenotype in our RNF185 KD studies.

As a ubiquitin ligase, RNF185 was previously associated with cancer cell migration. Lower level of RNF185 expression was found in glioblastoma (GBM), which inversely correlated with prognosis (19). RNF185 overexpression in a GBM cell line was sufficient to decrease cell migration *in vitro* (19). On the other hand, RNF185 was shown to contribute to gastric cancer metastasis through ubiquitination and proteasomal degradation of JWA, a microtubule-associated protein involved in the DNA damage response (18). Furthermore, RNF185 was identified as part of a ubiquitin-related gene signature that can be used to predict prostate cancer progression (65). However, how RNF185 downregulation triggers changes that may result in enhanced metastasis was not known. Our data suggest that reduced RNF185 levels induce activities that enhance EMT, which in turn impacts metastasis. Transcriptional mapping of clinical samples and RNAseq analysis of RNF185-depleted mouse prostate cancer lines identified genes implicated in cell adhesion, cytoskeleton remodeling, ECM structural regulation, and cancer cell migration. Among those, COL5A2 and COL3A1 are reportedly often overexpressed in cancers (21, 22). Collagen is a key component of the tumor microenvironment; thus, collagen dysregulation may underlie the tumor-intrinsic propensity to metastasize. COL5A2 was previously shown to promote proliferation and migration in prostate cancer lines, and its levels positively correlate with Gleason grade in PCa patients (66). COL5A2 is also upregulated and involved in tumor progression in colorectal cancer (67). COL3A1 was found to be a prognostic biomarker for ovarian carcinoma, breast cancer, and colorectal carcinoma (24–26, 68). Our studies reveal that upregulation of COL3A1 alone is sufficient to drive enhanced migration phenotypes seen in mouse and human prostate cancer cells.

How RNF185 controls COL3A1 expression remains to be determined. Our observations suggest a cross-talk between COL3A1 and COL5A2 transcription. Both genes are located within the same gene cluster on chromosome 2 and are often co-expressed and deregulated in connective tissue diseases (69–71). Their transcription has been reported to be controlled by TGF-β signaling, which has been implicated in metastasis of advanced stages of prostate cancer (72–75). Interestingly, TGFBi (TGF-β-induced) was one of the 13 common genes enriched in TCGA-PRAD patients with low RNF185 and in RNF185 KD MPC3 cells from our GSEA results (Fig, 3D, Sup. Fig. 3B). Other than TGFBi, COL3A1, and COL5A2, only ACTA2 was seen to be upregulated (Sup. Fig. 3C). While other known TGF-β targets, such as TGFB1, FN1 and SERPINH1 were transcriptionally unchanged, our proteomics analysis of RNF185-KD cells revealed increased abundance of FN1 and SERPINH1 protein in cells depleted of RNF185 (Sup. Fig. 3E). Western blot analysis also revealed a slight increase in total SMAD2 abundance and a reduction in SMAD4 protein, which has been shown to be associated with tumorigenesis and metastasis (Sup. Fig. 3D) (76). These preliminary results imply that TGF-β may be involved in the regulatory changes induced by RNF185, a possibility that warrants further exploration. Correspondingly, upregulated COL3A1 expression coincides with decreased RNF185 expression in metastatic PCa, substantiating the clinical relevance of this newly identified regulatory axis for PCa progression and metastasis. Our results show that manipulating COL3A1 and RNF185 expression is sufficient to impact PCa cells migration and suggest that components of this regulatory pathway may serve as markers to predict outcome. Further, as inhibition of COL3A1 attenuates metastasis in cells with reduced RNF185 expression, targeting collagen

becomes an appealing consideration, which may provide the basis for future therapeutic evaluations in low RNF185 expressing advanced prostate tumors.

Supplementary Material

Refer to Web version on PubMed Central for supplementary material.

Acknowledgements

We thank members of the Ronai lab for discussion. We thank SBP shared resources, which is supported by P30CA030199 grant, for their help with the analyses (vivarium, FACS, and bioinformatics). Support by R35CA197465 (to ZAR) is gratefully acknowledged.

REFERENCES CITED

1. Rawla P Epidemiology of Prostate Cancer. World J Oncol. 2019;10(2):63–89. [PubMed: 31068988]
2. Siegel RL, Miller KD, Jemal A. Cancer statistics, 2019. CA Cancer J Clin. 2019;69(1):7–34. [PubMed: 30620402]
3. Rebello RJ, Oing C, Knudsen KE, Loeb S, Johnson DC, Reiter RE, et al. Prostate cancer. Nat Rev Dis Primers. 2021;7(1):9. [PubMed: 33542230]
4. Ku SY, Gleave ME, Beltran H. Towards precision oncology in advanced prostate cancer. Nat Rev Urol. 2019;16(11):645–54. [PubMed: 31591549]
5. Yau R, Rape M. The increasing complexity of the ubiquitin code. Nat Cell Biol. 2016;18(6):579–86. [PubMed: 27230526]
6. Rape M Ubiquitylation at the crossroads of development and disease. Nat Rev Mol Cell Biol. 2018;19(1):59–70. [PubMed: 28928488]
7. Senft D, Qi J, Ronai ZA. Ubiquitin ligases in oncogenic transformation and cancer therapy. Nat Rev Cancer. 2018;18(2):69–88. [PubMed: 29242641]
8. Jeon YJ, Khelifa S, Ratnikov B, Scott DA, Feng Y, Parisi F, et al. Regulation of glutamine carrier proteins by RNF5 determines breast cancer response to ER stress-inducing chemotherapies. Cancer Cell. 2015;27(3):354–69. [PubMed: 25759021]
9. Li Y, Tinoco R, Elmén L, Segota I, Xian Y, Fujita Y, et al. Gut microbiota dependent anti-tumor immunity restricts melanoma growth in Rnf5(−/−) mice. Nat Commun. 2019;10(1):1492. [PubMed: 30940817]
10. Khateb A, Deshpande A, Feng Y, Finlay D, Lee JS, Lazar I, et al. The ubiquitin ligase RNF5 determines acute myeloid leukemia growth and susceptibility to histone deacetylase inhibitors. Nat Commun. 2021;12(1):5397. [PubMed: 34518534]
11. Didier C, Broday L, Bhoumik A, Israeli S, Takahashi S, Nakayama K, et al. RNF5, a RING finger protein that regulates cell motility by targeting paxillin ubiquitination and altered localization. Mol Cell Biol. 2003;23(15):5331–45. [PubMed: 12861019]
12. Iioka H, Iemura S, Natsume T, Kinoshita N. Wnt signalling regulates paxillin ubiquitination essential for mesodermal cell motility. Nat Cell Biol. 2007;9(7):813–21. [PubMed: 17558393]
13. Morito D, Hirao K, Oda Y, Hosokawa N, Tokunaga F, Cyr DM, et al. Gp78 cooperates with RMA1 in endoplasmic reticulum-associated degradation of CFTRDeltaF508. Mol Biol Cell. 2008;19(4):1328–36. [PubMed: 18216283]
14. Younger JM, Chen L, Ren HY, Rosser MF, Turnbull EL, Fan CY, et al. Sequential quality-control checkpoints triage misfolded cystic fibrosis transmembrane conductance regulator. Cell. 2006;126(3):571–82. [PubMed: 16901789]
15. El Khouri E, Le Pavec G, Toledano MB, Delaunay-Moisan A. RNF185 is a novel E3 ligase of endoplasmic reticulum-associated degradation (ERAD) that targets cystic fibrosis transmembrane conductance regulator (CFTR). J Biol Chem. 2013;288(43):31177–91. [PubMed: 24019521]

16. Kuang E, Okumura CY, Sheffy-Levin S, Varsano T, Shu VC, Qi J, et al. Regulation of ATG4B stability by RNF5 limits basal levels of autophagy and influences susceptibility to bacterial infection. PLoS Genet. 2012;8(10):e1003007. [PubMed: 23093945]
17. Tang F, Wang B, Li N, Wu Y, Jia J, Suo T, et al. RNF185, a novel mitochondrial ubiquitin E3 ligase, regulates autophagy through interaction with BNIP1. PLoS One. 2011;6(9):e24367. [PubMed: 21931693]
18. Qiu D, Wang Q, Wang Z, Chen J, Yan D, Zhou Y, et al. RNF185 modulates JWA ubiquitination and promotes gastric cancer metastasis. Biochim Biophys Acta Mol Basis Dis. 2018;1864(5 Pt A):1552–61. [PubMed: 29481911]
19. Lin K, Shen SH, Lu F, Zheng P, Wu S, Liao J, et al. CRISPR screening of E3 ubiquitin ligases reveals Ring Finger Protein 185 as a novel tumor suppressor in glioblastoma repressed by promoter hypermethylation and miR-587. J Transl Med. 2022;20(1):96. [PubMed: 35183197]
20. Ricard-Blum S The collagen family. Cold Spring Harb Perspect Biol. 2011;3(1):a004978. [PubMed: 21421911]
21. Myllyharju J, Kivirikko KI. Collagens and collagen-related diseases. Ann Med. 2001;33(1):7–21. [PubMed: 11310942]
22. Xu S, Xu H, Wang W, Li S, Li H, Li T, et al. The role of collagen in cancer: from bench to bedside. J Transl Med. 2019;17(1):309. [PubMed: 31521169]
23. De Martino D, Bravo-Cordero JJ. Collagens in Cancer: Structural Regulators and Guardians of Cancer Progression. Cancer Res. 2023;83(9):1386–92. [PubMed: 36638361]
24. Kuivaniemi H, Tromp G. Type III collagen (COL3A1): Gene and protein structure, tissue distribution, and associated diseases. Gene. 2019;707:151–71. [PubMed: 31075413]
25. Zhang H, Ding C, Li Y, Xing C, Wang S, Yu Z, et al. Data mining-based study of collagen type III alpha 1 (COL3A1) prognostic value and immune exploration in pan-cancer. Bioengineered. 2021;12(1):3634–46. [PubMed: 34252356]
26. Xiong G, Deng L, Zhu J, Rychahou PG, Xu R. Prolyl-4-hydroxylase α subunit 2 promotes breast cancer progression and metastasis by regulating collagen deposition. BMC Cancer. 2014;14:1. [PubMed: 24383403]
27. Engqvist H, Parris TZ, Kovács A, Nemes S, Werner Rönnerman E, De Lara S, et al. Immunohistochemical validation of COL3A1, GPR158 and PITHD1 as prognostic biomarkers in early-stage ovarian carcinomas. BMC Cancer. 2019;19(1):928. [PubMed: 31533654]
28. Zhou J, Yang Y, Zhang H, Luan S, Xiao X, Li X, et al. Overexpressed COL3A1 has prognostic value in human esophageal squamous cell carcinoma and promotes the aggressiveness of esophageal squamous cell carcinoma by activating the NF-κB pathway. Biochem Biophys Res Commun. 2022;613:193–200. [PubMed: 35598375]
29. Shen Y, Li X, Wang D, Zhang L, Li X, Su L, et al. COL3A1: Potential prognostic predictor for head and neck cancer based on immune-microenvironment alternative splicing. Cancer Med. 2023;12(4):4882–94. [PubMed: 36039012]
30. Gao YF, Mao XY, Zhu T, Mao CX, Liu ZX, Wang ZB, et al. COL3A1 and SNAP91: novel glioblastoma markers with diagnostic and prognostic value. Oncotarget. 2016;7(43):70494–503. [PubMed: 27655637]
31. Januchowski R, Świerczewska M, Sterzyńska K, Wojtowicz K, Nowicki M, Zabel M. Increased Expression of Several Collagen Genes is Associated with Drug Resistance in Ovarian Cancer Cell Lines. J Cancer. 2016;7(10):1295–310. [PubMed: 27390605]
32. Xu W, Li Z, Zhu X, Xu R, Xu Y. miR-29 Family Inhibits Resistance to Methotrexate and Promotes Cell Apoptosis by Targeting COL3A1 and MCL1 in Osteosarcoma. Med Sci Monit. 2018;24:8812–21. [PubMed: 30518744]
33. Wang L, Sun Y, Guo Z, Liu H. COL3A1 Overexpression Associates with Poor Prognosis and Cisplatin Resistance in Lung Cancer. Balkan Med J. 2022;39(6):393–400. [PubMed: 36148899]
34. Shi Y, Zheng C, Jin Y, Bao B, Wang D, Hou K, et al. Reduced Expression of METTL3 Promotes Metastasis of Triple-Negative Breast Cancer by m6A Methylation-Mediated COL3A1 Up-Regulation. Front Oncol. 2020;10:1126. [PubMed: 32766145]

35. Gao YF, Zhu T, Chen J, Liu L, Ouyang R. Knockdown of collagen α-1(III) inhibits glioma cell proliferation and migration and is regulated by miR128–3p. Oncol Lett. 2018;16(2):1917–23. [PubMed: 30008884]
36. Choi M, Chang CY, Clough T, Broudy D, Killeen T, MacLean B, et al. MSstats: an R package for statistical analysis of quantitative mass spectrometry-based proteomic experiments. Bioinformatics. 2014;30(17):2524–6. [PubMed: 24794931]
37. Ritchie ME, Phipson B, Wu D, Hu Y, Law CW, Shi W, et al. limma powers differential expression analyses for RNA-sequencing and microarray studies. Nucleic Acids Res. 2015;43(7):e47. [PubMed: 25605792]
38. Martin M Cutadapt removes adapter sequences from high-throughput sequencing reads. 2011. 2011;17(1):3.
39. Dobin A, Davis CA, Schlesinger F, Drenkow J, Zaleski C, Jha S, et al. STAR: ultrafast universal RNA-seq aligner. Bioinformatics. 2013;29(1):15–21. [PubMed: 23104886]
40. Li B, Dewey CN. RSEM: accurate transcript quantification from RNA-Seq data with or without a reference genome. BMC Bioinformatics. 2011;12:323. [PubMed: 21816040]
41. Ewels P, Magnusson M, Lundin S, Käller M. MultiQC: summarize analysis results for multiple tools and samples in a single report. Bioinformatics. 2016;32(19):3047–8. [PubMed: 27312411]
42. Love MI, Huber W, Anders S. Moderated estimation of fold change and dispersion for RNA-seq data with DESeq2. Genome Biol. 2014;15(12):550. [PubMed: 25516281]
43. Robinson MD, McCarthy DJ, Smyth GK. edgeR: a Bioconductor package for differential expression analysis of digital gene expression data. Bioinformatics. 2010;26(1):139–40. [PubMed: 19910308]
44. Lawrence M, Huber W, Pagès H, Aboyoun P, Carlson M, Gentleman R, et al. Software for computing and annotating genomic ranges. PLoS Comput Biol. 2013;9(8):e1003118. [PubMed: 23950696]
45. Subramanian A, Tamayo P, Mootha VK, Mukherjee S, Ebert BL, Gillette MA, et al. Gene set enrichment analysis: a knowledge-based approach for interpreting genome-wide expression profiles. Proc Natl Acad Sci U S A. 2005;102(43):15545–50. [PubMed: 16199517]
46. Taylor BS, Schultz N, Hieronymus H, Gopalan A, Xiao Y, Carver BS, et al. Integrative genomic profiling of human prostate cancer. Cancer Cell. 2010;18(1):11–22. [PubMed: 20579941]
47. Hoadley KA, Yau C, Hinoue T, Wolf DM, Lazar AJ, Drill E, et al. Cell-of-Origin Patterns Dominate the Molecular Classification of 10,000 Tumors from 33 Types of Cancer. Cell. 2018;173(2):291–304.e6. [PubMed: 29625048]
48. Cerami E, Gao J, Dogrusoz U, Gross BE, Sumer SO, Aksoy BA, et al. The cBio cancer genomics portal: an open platform for exploring multidimensional cancer genomics data. Cancer Discov. 2012;2(5):401–4. [PubMed: 22588877]
49. Perez-Riverol Y, Bai J, Bandla C, García-Seisdedos D, Hewapathirana S, Kamatchinathan S, et al. The PRIDE database resources in 2022: a hub for mass spectrometry-based proteomics evidences. Nucleic Acids Res. 2022;50(D1):D543–d52. [PubMed: 34723319]
50. Cunningham D, Zhang Q, Liu S, Parajuli KR, Nie Q, Ma L, et al. Interleukin-17 promotes metastasis in an immunocompetent orthotopic mouse model of prostate cancer. Am J Clin Exp Urol. 2018;6(3):114–22. [PubMed: 30038943]
51. Chen Z, Trotman LC, Shaffer D, Lin HK, Dotan ZA, Niki M, et al. Crucial role of p53-dependent cellular senescence in suppression of Pten-deficient tumorigenesis. Nature. 2005;436(7051):725–30. [PubMed: 16079851]
52. Foster BA, Gingrich JR, Kwon ED, Madias C, Greenberg NM. Characterization of prostatic epithelial cell lines derived from transgenic adenocarcinoma of the mouse prostate (TRAMP) model. Cancer Res. 1997;57(16):3325–30. [PubMed: 9269988]
53. Watson PA, Ellwood-Yen K, King JC, Wongvipat J, Lebeau MM, Sawyers CL. Context-dependent hormone-refractory progression revealed through characterization of a novel murine prostate cancer cell line. Cancer Res. 2005;65(24):11565–71. [PubMed: 16357166]
54. Jamaspishvili T, Berman DM, Ross AE, Scher HI, De Marzo AM, Squire JA, et al. Clinical implications of PTEN loss in prostate cancer. Nat Rev Urol. 2018;15(4):222–34. [PubMed: 29460925]

55. Imada EL, Sanchez DF, Dinalankara W, Vidotto T, Ebot EM, Tyekucheva S, et al. Transcriptional landscape of PTEN loss in primary prostate cancer. BMC Cancer. 2021;21(1):856. [PubMed: 34311724]
56. Liberzon A, Birger C, Thorvaldsdóttir H, Ghandi M, Mesirov JP, Tamayo P. The Molecular Signatures Database (MSigDB) hallmark gene set collection. Cell Syst. 2015;1(6):417–25. [PubMed: 26771021]
57. Kaneko M, Iwase I, Yamasaki Y, Takai T, Wu Y, Kanemoto S, et al. Genome-wide identification and gene expression profiling of ubiquitin ligases for endoplasmic reticulum protein degradation. Sci Rep. 2016;6:30955. [PubMed: 27485036]
58. van de Weijer ML, Krshnan L, Liberatori S, Guerrero EN, Robson-Tull J, Hahn L, et al. Quality Control of ER Membrane Proteins by the RNF185/Membralin Ubiquitin Ligase Complex. Mol Cell. 2020;79(5):768–81.e7. [PubMed: 32738194]
59. Tong CCL, Koptyra M, Raman P, Rathi KS, Choudhari N, Lin X, et al. Targeted gene expression profiling of inverted papilloma and squamous cell carcinoma. Int Forum Allergy Rhinol. 2022;12(2):200–9. [PubMed: 34510780]
60. Javanshir HT, Malekraeisi MA, Ebrahimi SSS, Bereimipour A, Kashani SF, Bostaki AA, et al. Investigation of key signaling pathways and appropriate diagnostic biomarkers selection between non-invasive to invasive stages in pancreatic cancer: a computational observation. J Med Life. 2022;15(9):1143–57. [PubMed: 36415513]
61. Wang Y, Gu W, Wen W, Zhang X. SERPINH1 is a Potential Prognostic Biomarker and Correlated With Immune Infiltration: A Pan-Cancer Analysis. Front Genet. 2021;12:756094. [PubMed: 35058967]
62. Tian S, Peng P, Li J, Deng H, Zhan N, Zeng Z, et al. SERPINH1 regulates EMT and gastric cancer metastasis via the Wnt/β-catenin signaling pathway. Aging (Albany NY). 2020;12(4):3574–93. [PubMed: 32091407]
63. Zhang H, Yan X, Gu H, Xue Q, Liu X. High SERPINH1 expression predicts poor prognosis in lung adenocarcinoma. J Thorac Dis. 2022;14(12):4785–802. [PubMed: 36647484]
64. Robinson D, Van Allen EM, Wu YM, Schultz N, Lonigro RJ, Mosquera JM, et al. Integrative clinical genomics of advanced prostate cancer. Cell. 2015;161(5):1215–28. [PubMed: 26000489]
65. Song G, Zhang Y, Li H, Liu Z, Song W, Li R, et al. Identification of a Ubiquitin Related Genes Signature for Predicting Prognosis of Prostate Cancer. Front Genet. 2021;12:778503. [PubMed: 35111198]
66. Ren X, Chen X, Fang K, Zhang X, Wei X, Zhang T, et al. COL5A2 Promotes Proliferation and Invasion in Prostate Cancer and Is One of Seven Gleason-Related Genes That Predict Recurrence-Free Survival. Front Oncol. 2021;11:583083. [PubMed: 33816226]
67. Wang J, Jiang YH, Yang PY, Liu F. Increased Collagen Type V α2 (COL5A2) in Colorectal Cancer is Associated with Poor Prognosis and Tumor Progression. Onco Targets Ther. 2021;14:2991–3002. [PubMed: 33981148]
68. Wang XQ, Tang ZX, Yu D, Cui SJ, Jiang YH, Zhang Q, et al. Epithelial but not stromal expression of collagen alpha-1(III) is a diagnostic and prognostic indicator of colorectal carcinoma. Oncotarget. 2016;7(8):8823–38. [PubMed: 26741506]
69. Cutting GR, McGinniss MJ, Kasch LM, Tsipouras P, Antonarakis SE. Physical mapping by PFGE localizes the COL3A1 and COL5A2 genes to a 35-kb region on human chromosome 2. Genomics. 1990;8(2):407–10. [PubMed: 1979060]
70. Kempers MJ, Wessels M, Van Berendoncks A, van de Laar IM, de Leeuw N, Loeys B. Phenotype of COL3A1/COL5A2 deletion patients. Eur J Med Genet. 2022;65(10):104593. [PubMed: 35964930]
71. Meienberg J, Rohrbach M, Neuenschwander S, Spanaus K, Giunta C, Alonso S, et al. Hemizygous deletion of COL3A1, COL5A2, and MSTN causes a complex phenotype with aortic dissection: a lesson for and from true haploinsufficiency. Eur J Hum Genet. 2010;18(12):1315–21. [PubMed: 20648054]
72. Bertelli R, Valenti F, Oleggini R, Caridi G, Altieri P, Coviello DA, et al. Cell-specific regulation of alpha1(III) and alpha2(V) collagen by TGF-beta1 in tubulointerstitial cell models. Nephrol Dial Transplant. 1998;13(3):573–9. [PubMed: 9550630]

73. Ilieș RF, Aioanei CS, Cătană A, Halmagyi SR, Lukacs I, Tokes RE, et al. Involvement of COL5A2 and TGF-β1 in pathological scarring. Exp Ther Med. 2021;22(4):1067. [PubMed: 34447460]

74. Xie F, Ling L, van Dam H, Zhou F, Zhang L. TGF-β signaling in cancer metastasis. Acta Biochim Biophys Sin (Shanghai). 2018;50(1):121–32. [PubMed: 29190313]

75. Thompson-Elliott B, Johnson R, Khan SA. Alterations in TGFβ signaling during prostate cancer progression. Am J Clin Exp Urol. 2021;9(4):318–28. [PubMed: 34541030]

76. Ding Z, Wu CJ, Chu GC, Xiao Y, Ho D, Zhang J, et al. SMAD4-dependent barrier constrains prostate cancer growth and metastatic progression. Nature. 2011;470(7333):269–73. [PubMed: 21289624]

Implications

RNF185 is identified as an important regulator of prostate cancer migration and metastasis, in part due to its regulation of COL3A1. Both RNF185 and COL3A1 may serve as novel markers for prostate tumors.

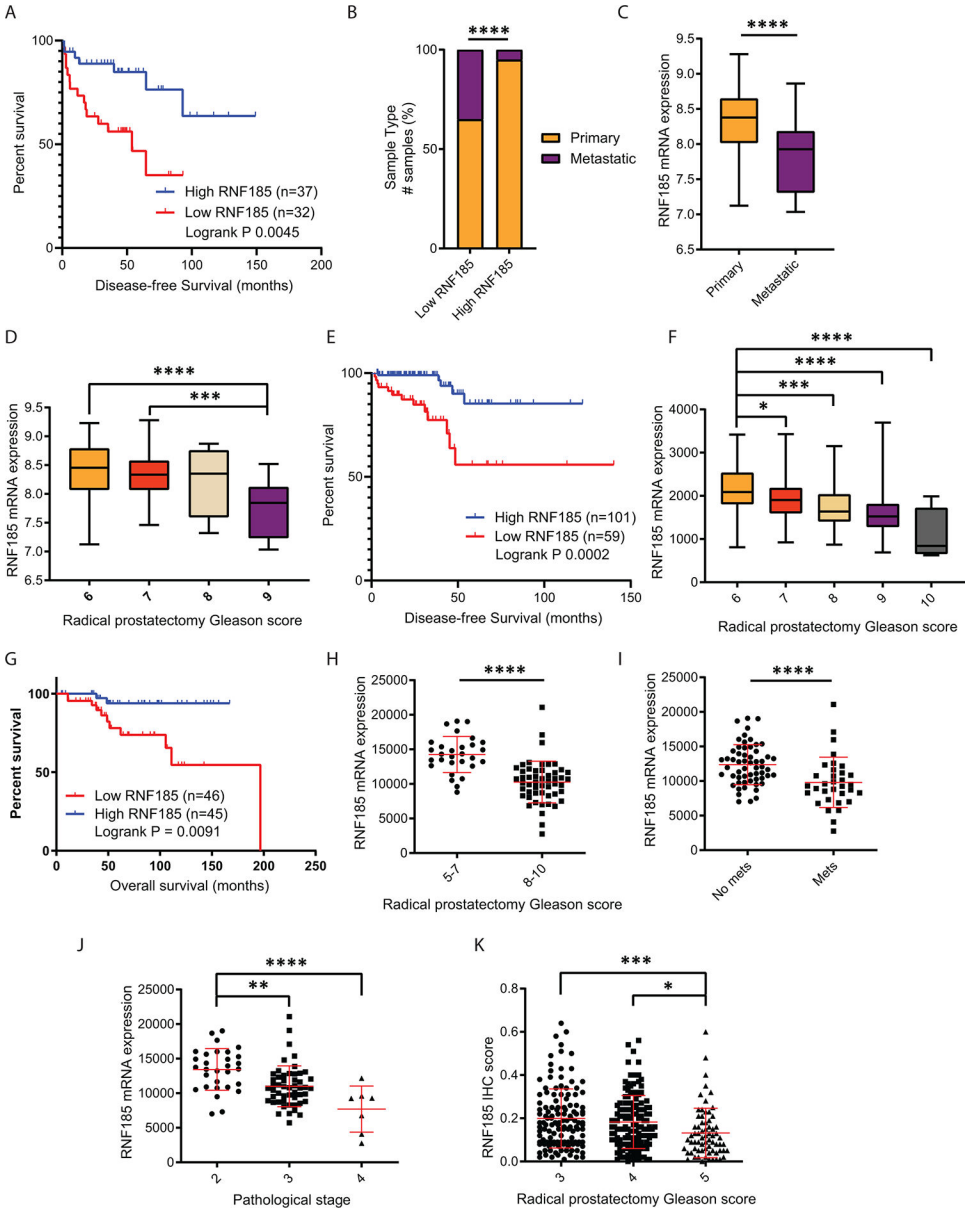

Fig. 1. RNF185 expression correlates with metastatic load and PCa patient outcome.

(A) Disease-free survival in PCa samples stratified by RNF185 mRNA expression ("Low RNF185" = bottom quartile; "High RNF185" = top quartile). (B) Proportion of sample types in Low RNF185 vs. High RNF185. (C) RNA-seq analysis of RNF185 mRNA in primary tumors (n=131) and metastasis (n=19). (D) RNA-seq analysis of RNF185 mRNA in samples sorted by Gleason score (6: n=41; 7: n=76; 8: n=11; 9: n=11). (E) Disease-free survival in samples stratified by RNF185 mRNA expression using the same cutoffs as in (A). (F) RNA-seq analysis of RNF185 in samples sorted by Gleason score (6: n=45; 7: n=247; 8: n=64; 9: n=138; 10: n=4). (G) Overall survival in PCa samples stratified by RNF185 mRNA expression using the median as cutoffs. (H) RNA-seq analysis of RNF185 in samples sorted by Gleason score (5–7: n=29; 8–10: n=52). (I) RNA-seq analysis of RNF185 in patients with (n=33) and without (n=58) metastases. (J) RNA-seq analysis of RNF185 in samples sorted

by pathological stages (2: n=30; 3: n=51; 4: n=7). (K) RNF185 IHC staining score in PCa TMA stratified by Gleason groups (3: n=127; 4: n=133; 5: n=69). (A-D) generated using datasets from Taylor et al. (46); (E-F) generated using The Cancer Genome Atals' (TCGA) Pan-Cancer Atlas and Firehose legacy Prostate Adenocarcinoma (PRAD) datasets. (G-K) generated from VPC independent cohorts. Box plots show the median and whiskers (min to max), scatter plots show mean with SD. *P < 0.05, **P < 0.005, ***P < 0.001, ****P < 0.0001 by two-tailed t-test, Mann-Whitney u test, one-way ANOVA or Fisher's exact test (B). Survival graphs used the Kaplan–Meier with a log-rank (Mantel-Cox).

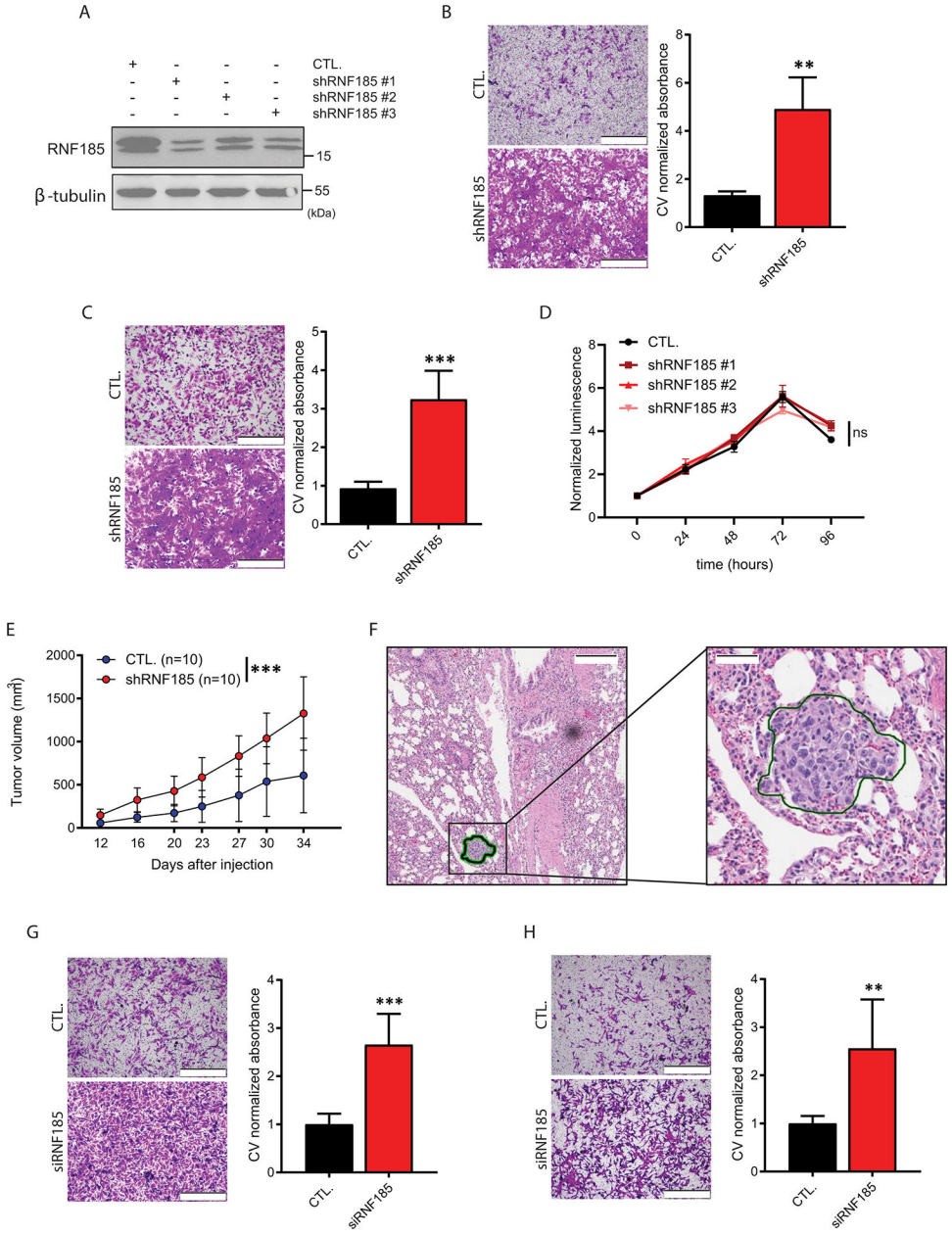

Fig. 2. RNF185 KD enhances PCa migration, tumor development and metastatic load.

(A) Western blot analysis of RNF185 protein levels in lysates of MPC3 cells stably expressing the indicated vectors. (B) Representative pictures of migrated MPC3 cells expressing the indicated vectors and quantification of migrated cells based on Crystal Violet (CV) absorbance. (C) Representative images of MPC3 cells expressing the indicated vectors that migrate through Matrigel and quantification of those migrated cells based on Crystal Violet absorbance. (D) Proliferation assay of the same cells shown in (A). (E) Growth of MPC3-pLKO and MPC3-shRNF185 cells after subcutaneous injection of 5×10^5 cells into the flank of NSG mice (n=10/group). (F) Representative H&E staining of lung metastasis from mice inoculated with MPC3-shRNF185 cells (34 days post-injection). (G) Representative images of migrated PC3 cells transfected with siRNF185 or Universal

negative control and quantification of migrated cells based on Crystal Violet (CV) staining absorbance. (H) Representative images of migrated C4–2B cells transfected with siRNF185 or Universal negative control and quantification of migrated cells based on Crystal Violet (CV) absorbance. Box plots show the median and whiskers (min to max). Growth curve shows the mean and whiskers (min to max). Box plots show median and whiskers. **P < 0.005, ***P < 0.001, ****P < 0.0001 by two-tailed t-test or two-way ANOVA.

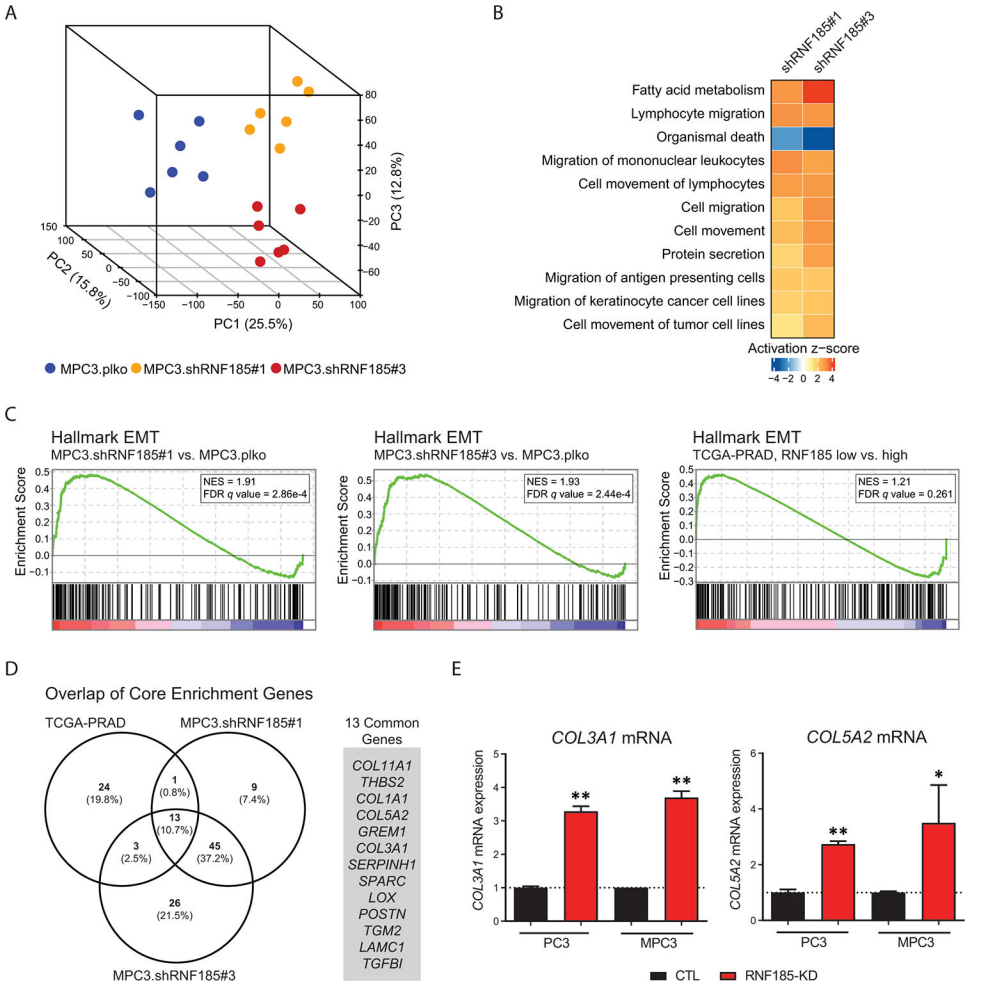

Fig. 3. Transcriptional analysis of RNF185 KD MPC3 cells and comparison analysis with clinical transcriptomics reveals EMT pathway activation and collagen upregulation.

(A) Principal Component Analysis (PCA) plot of MPC3-pLKO and MPC3-shRNF185 #1 and #3 biological replicates. (B) Heatmap comparing significantly altered diseases and functions in MPC3-shRNF185 #1 and #3 compared to MPC3-pLKO. (C) GSEA enrichment plots showing enrichment of the EMT hallmark gene set in MPC3-shRNF185 #1 and #3 relative to MPC3-pLKO, and in TCGA's PRAD patients with low RNF185 mRNA expression (bottom 25%) relative to those with high expression (top 25%). (D) Venn Diagrams of enriched genes from HALLMARK_EMT in MPC3-shRNF185 #1 and #3 cells and in low RNF185 expressing patients from TCGA dataset. (E) qRT-PCR analysis of COL5A2 and COL3A1 in MPC3-pLKO and MPC3-shRNF185 cells, and in the human prostate cancer line PC3 transfected with RNF185 siRNA. Box plots show median and whiskers.

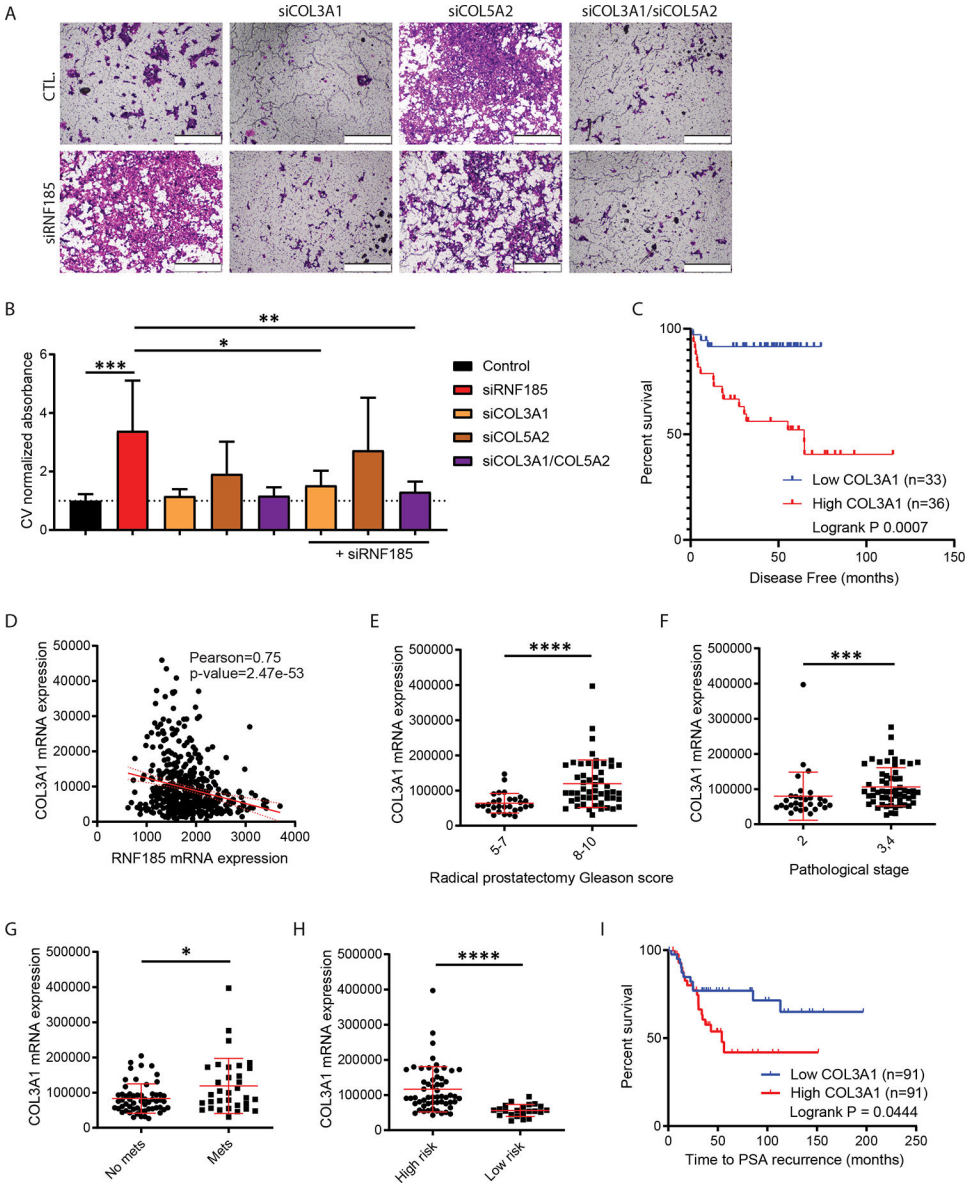

Fig. 4. COL3A1 depletion in RNF185-deficient PC3 cells rescues migration advantage conferred by RNF185 KD alone.

(A) Representative images of migrated PC3 cells transfected with the indicated siRNAs. (B) Quantification of migrated cells based on Crystal Violet (CV) absorbance. (C) Disease-free survival in samples stratified by COL3A1 mRNA expression ("Low COL3A1" = bottom quartile; "High COL3A1" = top quartile). (D) Scatter plot of RNF185 and COL3A1 mRNA expression in PCa patients (Pearson correlation=0.75, p-value=2.47e-53). (E) RNA-seq analysis of COL3A1 in samples sorted by Gleason score (5–7: n=29; 8–10: n=52). (F) RNA-seq analysis of COL3A1 in samples sorted by pathological stages (2: n=30; 3,4: n=58). (G) RNA-seq analysis of COL3A1 in patients with (n=33) and without (n=58) metastases. (H) RNA-seq analysis of COL3A1 in samples sorted by their chances of recurrence (High risk; n=57, Low risk: n=22). (I) PSA-recurrence survival in samples stratified by COL3A1 mRNA expression ("Low COL3A1" = bottom quartile; "High COL3A1" = top quartile). (C)

generated using datasets from Taylor et al. (46) (D) generated using TCGA PRAD dataset. (E-I) generated using VPC dataset. Box plots show the median and whiskers (min to max), scatter plots show mean with SD. *P < 0.05, **P < 0.005, ***P < 0.001, ****P < 0.0001 by Mann-Whitney u test or one-way ANOVA. Survival graphs used the Kaplan–Meier with a log-rank (Mantel-Cox).

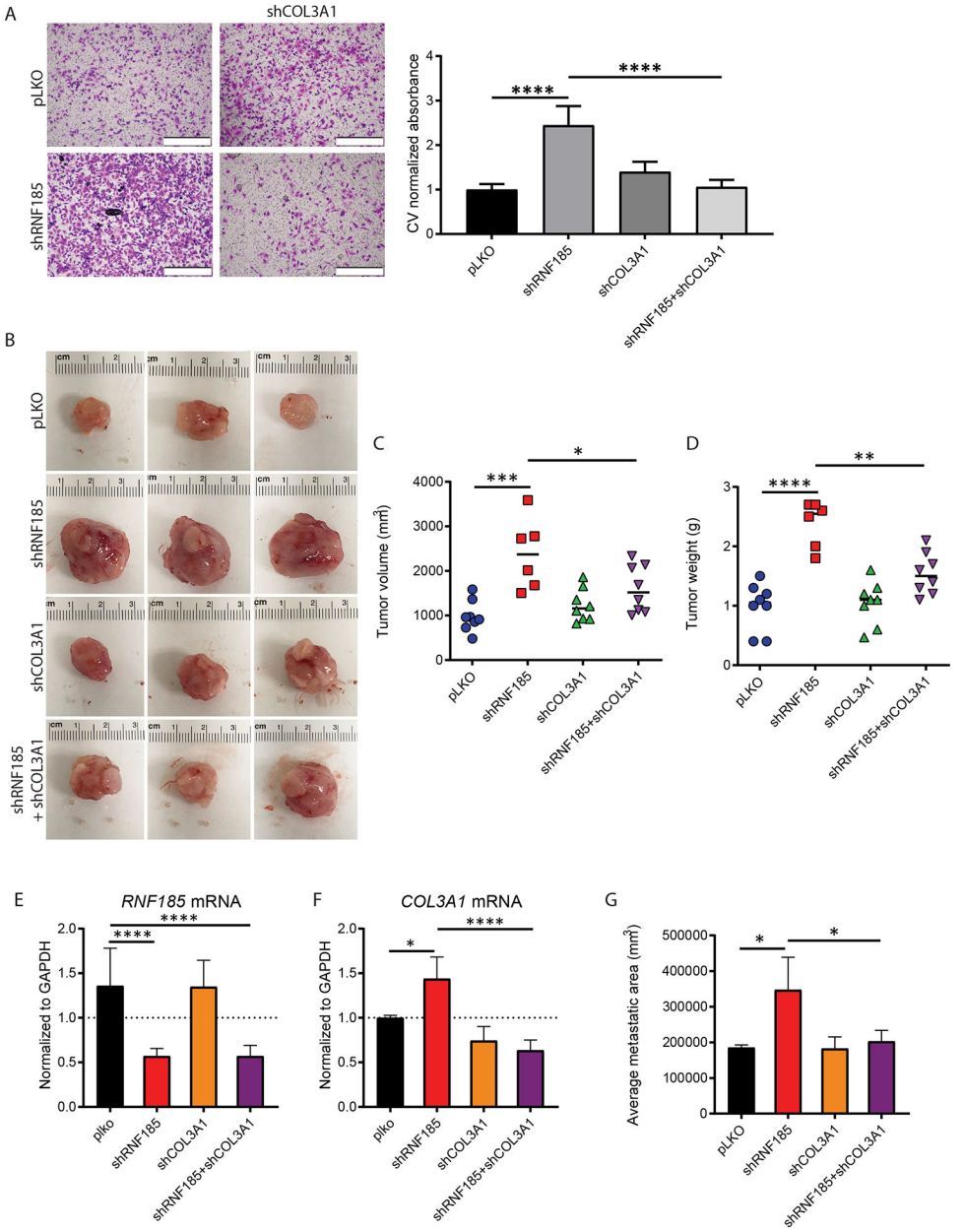

Fig. 5. COL3A1 depletion in RNF185-deficient MPC3 cells rescues tumor growth advantage and metastatic propensity conferred by RNF185 KD alone in subcutaneous grafts.

(A) Representative images of MPC3 cells expressing the indicated vectors that migrated through Matrigel and quantification of migrated cells based on Crystal Violet (CV) absorbance. (B) Representative pictures of resected tumors originating from cells expressing the indicated vectors. (C) Volume of resected tumors originating from cells expressing the indicated vectors 28 days after subcutaneous injection (n=6–8/group). (D) Weights of resected tumors originating from cells expressing the indicated vectors 28 days after subcutaneous injection (n=6–8/group). (E) qRT-PCR analysis of RNF185 mRNA in tumors emerging following subcutaneous injection of either MPC3.plko, MPC3.shRNF185, MPC3.COL3A1 or MPC3.shRNF185+shCOL3A1 cells into flanks of NSG mice. (F) qRT-

PCR analysis of COL3A1 mRNA in tumors emerging following subcutaneous injection of either MPC3.plko, MPC3.shRNF185, MPC3.COL3A1 or MPC3.shRNF185+shCOL3A1 cells into flanks of NSG mice. (G) Average metastatic area (mm^3) per section, measured in 9 serial sections of the lungs for each mouse within each group (n=6–8 mice per group). Scatter plots show the mean with SD, box plots show median with whiskers (min to max). *P < 0.05, **P < 0.005, ***P < 0.001, ****P < 0.0001 by one-way ANOVA.